

Investigating Lorentz Violation with the long baseline experiment P2O

Nishat Fiza,^{1,*} Nafis Rezwan Khan Chowdhury,^{2,†} and Mehedi Masud^{3,‡}

¹*Department of Physical Sciences, IISER Mohali,*

Knowledge City, SAS Nagar, Mohali - 140306, Punjab, India

²*Institut de Física Corpuscular (CSIC-Universitat de València), Parc Científic de la UV*

C/ Catedrático José Beltrán, 2, E-46980 Paterna (València), Spain

³*Center for Theoretical Physics of the Universe,*

Institute for Basic Science (IBS), Daejeon 34126, Korea

One of the basic proposition of quantum field theory is Lorentz invariance. The spontaneous breaking of Lorentz symmetry at a more fundamental theory at high energy scale can manifest itself at the low energy extension of standard model perturbatively via effective field theories. The present and future Long-baseline neutrino experiments can give a scope to observe such a Planck-suppressed physics of Lorentz Invariance Violation. The proposed long baseline experiment P2O extending from Protvino to ORCA with a baseline of 2595 km, is expected to provide good sensitivities to unresolved issues, especially neutrino mass ordering. P2O can offer good statistics even with a moderate beam power and runtime, owing to the very large (~ 6 Mt) detector volume at ORCA. Here we discuss in detail how the individual LIV parameters affect neutrino oscillation at the P2O and DUNE baseline at the level of probability and derive analytical expressions to understand interesting degeneracies and other features. We estimate $\Delta\chi^2$ sensitivities to the LIV parameters, analyzing their correlations among each other, and also with the standard oscillation parameters. We calculate these results for P2O alone and also carry out a combined analysis of P2O with DUNE. We point out crucial features in the sensitivity contours and explain them qualitatively with the help of the relevant probability expressions derived here. Finally we estimate constraints on the individual LIV parameters at a confidence level (C.L.) of 95% with the combined (P2O+DUNE) analysis and highlight the improvement over the existing constraints. We also find out that the additional degeneracy induced by the LIV parameter a_{ee} around -22×10^{-23} GeV is lifted by the combined analysis at 95% C.L.

* ph15039@iisermohali.ac.in

† nafis.chowdhury@ific.uv.es

‡ masud@ibs.re.kr

CONTENTS

I. Introduction	2
II. Theoretical background	5
III. Impact of LIV parameters on probability	6
IV. Simulation details	13
V. Correlations among the LIV parameters	15
VI. Degeneracies with the standard oscillation parameters	17
VII. Bounds on the LIV parameters	19
VIII. Summary and conclusion	20
Acknowledgement	22
References	23

I. INTRODUCTION

The phenomenon of neutrino oscillation which was first experimentally established more than twenty years back from the observations of atmospheric and solar neutrinos [1, 2] is one of the most transparent currently available portals into the rich physics beyond the standard model (BSM) of particle physics. In standard scenario neutrino oscillation is governed by six parameters, namely the three mixing angles ($\theta_{12}, \theta_{13}, \theta_{23}$); one Dirac CP phase (δ_{13}), and two mass-squared differences ($\Delta m_{21}^2, \Delta m_{31}^2$). So far $\theta_{12}, \theta_{23}, \Delta m_{21}^2$ and the magnitude $|\Delta m_{31}^2|$ have been measured with good precision from various neutrino experiments. One of the principal focus of the neutrino oscillation community is now on the measurement and implications of the values of the remaining parameters: the leptonic (Dirac) CP phase δ_{13} , the sign of Δm_{31}^2 (denoting the correct neutrino mass ordering) and the octant of the mixing angle θ_{23} . A value of δ_{13} not equal to zero or π would indicate CP violation in the lepton sector. This, in turn, can potentially shed light on the another fundamental puzzle, namely the baryon asymmetry of the universe [3]. Resolution of the correct mass ordering and octant can help narrow down the plausible set of models explaining neutrino mass generation.

Presently running long-baseline neutrino oscillation experiments Tokai to Kamioka (T2K) [4] and NuMI Off-axis ν_e Appearance (NO ν A) [5] are already giving us glimpses to the resolutions of the issues mentioned above. T2K data [6] has ruled out CP conservation ($\delta_{13} \simeq 0, \pi$) at 95% confidence limit (C.L.). Irrespective of the mass ordering, at 99.73% C.L. (3σ) T2K excludes 42% of the entire parameter space for δ_{13} (mostly around $+\pi/2$), restricting the allowed region to roughly $\delta_{13} \in [-\pi, 0.04\pi] \cup [0.89\pi, \pi]$. NO ν A data [7], on the other hand indicates a slight preference for θ_{23} lying in the higher octant (HO) at a C.L. of 1.6σ . It also excludes most of the choices near $\delta_{13} = \pi/2$ at a C.L. $\geq 3\sigma$ for inverted mass ordering (IO). These measurements are expected to become more accurate as more data pour in. Though the global analyses of neutrino data [8–11] shows an indication towards NO with θ_{23} possibly lying in the higher octant, the CP phase still has a large uncertainty.

In near future, various other next-generation neutrino experiments with more sophisticated detection technologies are expected to start taking data. These experiments include, among others, Deep Underground Neutrino Experiment (DUNE) [12, 13], Tokai to Hyper-Kamiokande (T2HK) [14], Tokai to Hyper-Kamiokande with a second detector in Korea (T2HKK) [15], European Spallation Source ν Super Beam (ESS ν SB) [16], Jiangmen Underground Neutrino Observatory (JUNO) [17], Protvino to ORCA (P2O) [18]. These experiments are expected to reach upto an unprecedented (\sim a few percent) level of precision in measuring the oscillation parameters and hence are also susceptible to the presence of various possible new physics.

CPT symmetry, one of the most sacred foundations in local relativistic quantum field theory, is based on the assumptions of the hermiticity of the hamiltonian, Lorentz Invariance and local commutativity. Since an interacting theory with CPT violation also breaks Lorentz Invariance [19], one widely used strategy to probe CPT violation is to analyze the associated Lorentz Invariance Violation (LIV). Spontaneous breakdown of Lorentz Violation may occur in theories of quantum gravity (in string theory, for *e.g.*) at Planck scale ($M_P \sim 10^{19}$ GeV), forcing a Lorentz tensor field to acquire a non-zero vacuum expectation value, thus selecting a preferred spacetime direction [20–24]. It has been shown in literature that the Standard Model (SM) of particle physics can be extended to construct a low energy effective field theory (EFT), namely Standard Model Extension (SME) [25–27] that includes such Lorentz-violating effects, suppressed by M_P . Neutrino oscillation by virtue of its interferometric nature, can probe such LIV effects at SME, thereby offering us a probe to the Planck scale physics.

A broad range of experimental parameters such as neutrino-beam flavor composition, length, direction, and energy, as well as detector techniques provide different and often complementary

sensitivities to the many higher dimensional operators characterizing LIV at accessible range of energies. Indeed, constraints on LIV parameters of SME have been obtained analysing the data from several neutrino experiments, - LSND [28], MINOS [29, 30], MiniBooNE [31], Double Chooz [32], Super-Kamiokande [33], T2K [34], IceCube [35]. Outside the experimental collaboration also, there exist studies to explore LIV and CPT-violation, - for *e.g.*, in long-baseline accelerator neutrinos [36–44], short-baseline reactor antineutrinos [45], atmospheric neutrinos [46–49], solar neutrinos [50], and high-energy astrophysical neutrinos [51–53]. For a comprehensive list of constraints on all the LIV parameters collected together we refer the readers to reference [54].

The proposed P2O experiment [18, 55–57] will have a baseline extending approximately 2595 km from the Protvino accelerator complex to the ORCA/KM3NET detector at the Mediterranean, - both of which are already existing. P2O baseline is most sensitive to first $\nu_\mu \rightarrow \nu_e$ oscillation maxima around 4-5 GeV. Neutrino interaction around this energy is dominated by Deep Inelastic Scattering which is relatively well described theoretically, compared to, for *e.g.*, 2-2.5 GeV (for DUNE) where resonant interactions and nuclear effects can potentially impact the measurements more significantly [58–63]. Such a very long baseline and relatively higher energy of the oscillation maxima gives P2O an excellent level of sensitivity, especially towards neutrino mass ordering. As has been illustrated in reference [64], the P2O baseline is favourable to determine mass hierarchy also due to the much less interference by the hierarchy-CP phase degeneracy. The very large detector volume of 6 Mt at ORCA will allow to detect thousands of neutrino events per year even with a very large baseline and a moderate beam power, - subsequently offering sensitivities to neutrino mass ordering, CP violation and θ_{23} -octant that are competitive with the current and upcoming long-baseline neutrino experiments¹ [18, 65]. In recent years, there has been some interests in estimating new physics capabilities of P2O. Reference [66] discussed the sensitivity reach of P2O to Non-unitarity of the leptonic mixing matrix and also estimated how it will affect the standard physics searches. The authors of [64] discussed about the possible optimization of P2O in order to explore non-standard neutrino interactions. In the present work, we analyze the capabilities of P2O to probe Lorentz and CPT violation and estimate the constraints that can be put on these new physics parameters.

The present manuscript is organised as follows. In Sec. II we briefly describe the formalism of LIV. In Sec. III we discuss in detail the probability expressions in presence of LIV parameters and provide a thorough analysis of the changes induced by each LIV parameter by means of heatplots.

¹ P2O in its nominal configuration with a 90 kW beam, can resolve mass ordering with $\gtrsim 6\sigma$ sensitivity in 5 years of running, and also has a projected sensitivity of more than 3σ to θ_{23} -octant with 3 years of running. With a 450 kW beam, it can offer 2σ sensitivity to δ_{13} after 3 years of operation.

Sec. IV describes the simulation procedures followed in this work. Secs. V and VI illustrate the $\Delta\chi^2$ sensitivity results showing the correlations of LIV parameters among themselves and with the standard oscillation parameters δ_{13} and θ_{23} . Sec. VII shows our final results as the constraints on LIV parameters obtained from this work, followed by the summary and conclusion in Sec. VIII.

II. THEORETICAL BACKGROUND

We follow the widely used formalism of introducing Planck-suppressed CPT/Lorentz violating effect to write a Lagrangian for the Standard Model Extension (SME), as developed in [25–27, 67–70]. The Lagrangian relevant for neutrino propagation in SME is then given by,

$$\mathcal{L} = \frac{1}{2}\bar{\Psi}(i\not{\partial} - M + \hat{Q})\Psi + h.c., \quad (1)$$

where Ψ is the spinor containing the neutrino fields. The first two terms inside the parentheses are the usual kinetic and the mass terms in the SM Lagrangian while the LIV effect has been incorporated by the operator \hat{Q} . The Lorentz-violating term, which is suppressed by Planck-mass scale M_P can be written in terms of the basis of the usual gamma-matrix algebra. Considering only renormalizable and only the CPT-violating LIV terms, one can write the LIV Lagrangian from Eq. 1 in terms of vector and pseudovectors [25],

$$\mathcal{L}_{\text{LIV}} \supset -\frac{1}{2} \left[a_{\alpha\beta}^{\mu} \bar{\psi}_{\alpha} \gamma_{\mu} \psi_{\beta} + b_{\alpha\beta}^{\mu} \bar{\psi}_{\alpha} \gamma_5 \gamma_{\mu} \psi_{\beta} \right], \quad (2)$$

where a_{μ}, b_{μ} are constant hermitian matrices and are in general combinations of tensor expectations, mass parameter and coefficients arising from the decomposition of gamma matrices. We focus on the following CPT-violating LIV parameter that is relevant in the context of the propagation of left handed neutrinos,

$$(a_L)_{\alpha\beta}^{\mu} = (a + b)_{\alpha\beta}^{\mu}. \quad (3)$$

Since our focus is on the isotropic component of the LIV terms, we will make the Lorentz indices zero. To further simplify our notation we will henceforth denote the parameter $(a_L)_{\alpha\beta}^0$ as $a_{\alpha\beta}$ ².

Using spinor redefinitions to get rid of the non-trivial time derivatives in the Lorentz-violating Lagrangian in Eq. 1 and carrying out some lengthy algebra with the resulting modified Dirac equation one can derive the Lorentz-violating effective hamiltonian relevant for ultrarelativistic,

² These components are defined in the Sun-centered celestial equatorial frame [68].

left-handed neutrino propagation through matter [69–71].

$$H \simeq \underbrace{\frac{1}{2E} U \begin{pmatrix} m_1^2 & 0 & 0 \\ 0 & m_2^2 & 0 \\ 0 & 0 & m_3^2 \end{pmatrix} U^\dagger}_{H_{\text{vac}}} + \underbrace{\sqrt{2} G_F N_e \begin{pmatrix} 1 & & \\ & 0 & \\ & & 0 \end{pmatrix}}_{H_{\text{mat}}} + \underbrace{\begin{pmatrix} a_{ee} & a_{e\mu} & a_{e\tau} \\ a_{e\mu}^* & a_{\mu\mu} & a_{\mu\tau} \\ a_{e\tau}^* & a_{\mu\tau}^* & a_{\tau\tau} \end{pmatrix}}_{H_{\text{LIV}}}. \quad (4)$$

The first term containing the usual leptonic mixing matrix U and the neutrino mass eigenstates $m_i (i = 1, 2, 3)$ is the standard vacuum hamiltonian. The second term, proportional to Fermi constant G_F and electron density N_e along the neutrino propagation, originates from standard charged-current coherent forward scattering of neutrinos with electrons in earth matter. The third term containing the LIV parameters $a_{\alpha\beta}$'s ($\alpha, \beta = e, \mu, \tau$) incorporates the effect of LIV (and also CPT-violation). The off-diagonal $a_{\alpha\beta}$'s ($\alpha \neq \beta$) are complex with a phase ($\varphi_{\alpha\beta}$) associated to them, while the diagonal parameters are real.

It is worthwhile to mention here that the physics of neutral current (NC) Nonstandard interaction (NSI) (usually denoted by $\varepsilon_{\alpha\beta}$) that arises from neutrino mass models and introduces couplings between the neutrinos and the first generation fermions e, u, d , has an apparent similarity with the form of LIV hamiltonian, - thereby suggesting a mathematical mapping: $\varepsilon_{\alpha\beta} \leftrightarrow a_{\alpha\beta}/\sqrt{2}G_F N_e$. But there is a crucial difference between these two different kinds of physics scenario as discussed in detail in reference [72]. NC NSI is proportional to the density along the neutrino trajectory and is thus very tiny for short-baseline neutrino experiments. LIV, on the other hand, is an intrinsic effect that is present even in the vacuum.

III. IMPACT OF LIV PARAMETERS ON PROBABILITY

In this work we focus on $a_{\alpha\beta}$'s and we will now describe how they affect the oscillation probability expressions in various channels. Since the main contribution comes from the $\nu_\mu \rightarrow \nu_e$ oscillation channel, we discuss about how $P(\nu_\mu \rightarrow \nu_e)$ is affected by LIV. The most important LIV parameters impacting this channel are $a_{e\mu}$ and $a_{e\tau}$, and also to a lesser extent a_{ee} . Following the similar approach as in reference [43, 73–75], we can approximately write the $\nu_\mu \rightarrow \nu_e$ oscillation probability as the sum of the following three terms,

$$P_{\mu e}(\text{SI+LIV}) \simeq P_{\mu e}(\text{SI}) + P_{\mu e}(a_{e\mu}) + P_{\mu e}(a_{e\tau}), \quad (5)$$

where the first term on the right hand side is the probability term corresponding to standard interaction (SI) with earth matter, while the other two terms come due to the presence of LIV

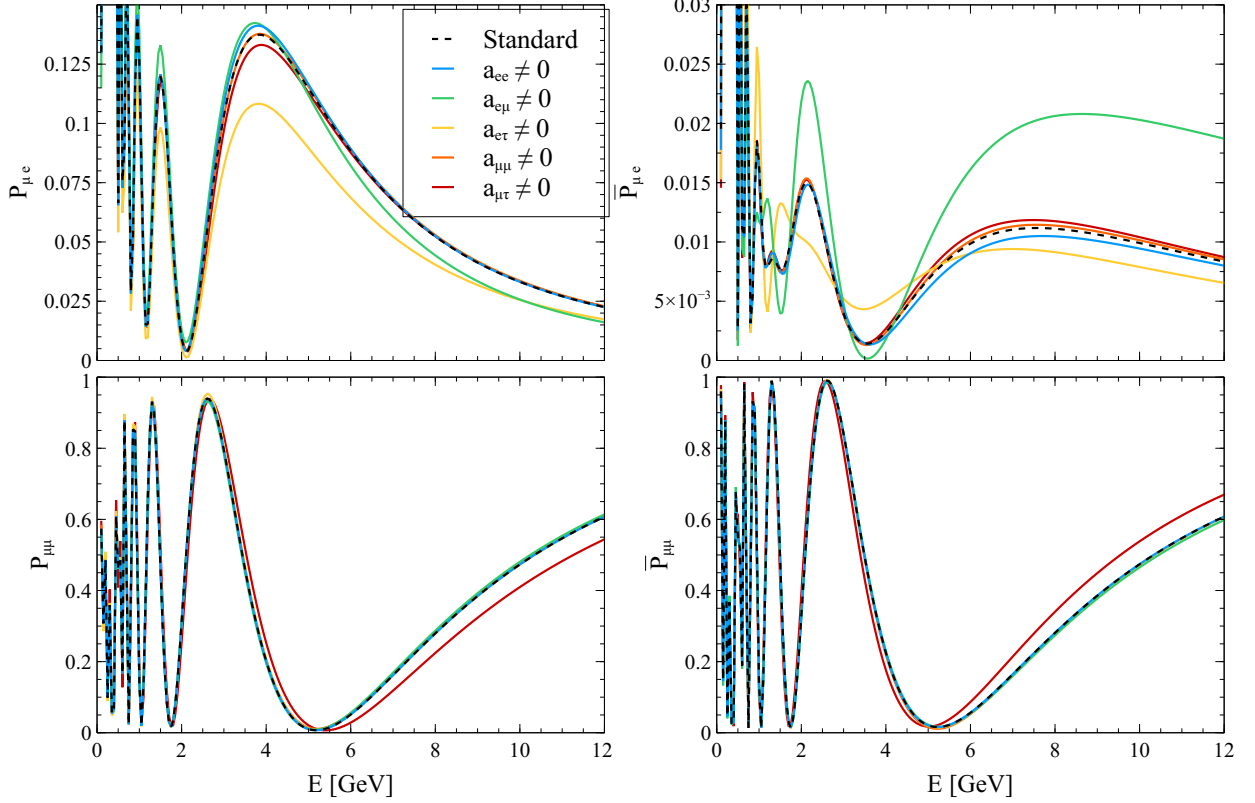


FIG. 1. The impact of individual LIV parameters on oscillation probability at the P2O baseline of 2595 km. The top (bottom) row shows the probability for appearance (disappearance) channel, while the left (right) column indicates the neutrino (anti-neutrino) mode. The black dotted curve shows the probability for the standard (no LIV) case, while the solid coloured curves are for individual LIV parameters present. The non-zero values of the individual LIV parameters $a_{\alpha\beta}$ was taken as 5×10^{-23} GeV, while the CP phase associated with the off-diagonal LIV parameters was taken as zero.

parameters $a_{e\mu}$ and $a_{e\tau}$. The three terms on the right hand side can be shown to have the following forms.

$$P_{\mu e}(\text{SI}) \simeq X + Y \cos(\delta_{13} + \Delta), \quad (6)$$

$$P_{\mu e}(a_{e\mu}) \simeq \frac{8|a_{e\mu}|E\Delta s_{13} \sin 2\theta_{23}c_{23} \sin \Delta}{\Delta m_{31}^2} \left[-\sin \Delta \sin(\delta_{13} + \varphi_{e\mu}) + \left(\frac{s_{23}^2}{c_{23}^2} \frac{\sin \Delta}{\Delta} + \cos \Delta \right) \cos(\delta_{13} + \varphi_{e\mu}) \right], \quad (7)$$

$$P_{\mu e}(a_{e\tau}) \simeq \frac{8|a_{e\tau}|E\Delta s_{13} \sin 2\theta_{23}s_{23} \sin \Delta}{\Delta m_{31}^2} \left[\sin \Delta \sin(\delta_{13} + \varphi_{e\tau}) + \left(\frac{\sin \Delta}{\Delta} - \cos \Delta \right) \cos(\delta_{13} + \varphi_{e\tau}) \right]. \quad (8)$$

The different familiar terms appearing in Eqs. 6, 7, 8 are given in the following.

$$\begin{aligned}
X &= 4s_{13}^2 c_{13}^2 s_{23}^2 \frac{\sin^2 [(1 - \hat{A})\Delta]}{(1 - \hat{A})^2}; & Y &= 8\alpha s_{12} c_{12} s_{23} c_{23} s_{13} c_{13} \frac{\sin \hat{A} \Delta \sin [(1 - \hat{A})\Delta]}{\hat{A} (1 - \hat{A})}, \\
\hat{A} &= \frac{2\sqrt{2}G_F N_e E}{\Delta m_{31}^2}; & \Delta &= \frac{\Delta m_{31}^2 L}{4E}; & s_{ij} &= \sin \theta_{ij}; & c_{ij} &= \cos \theta_{ij}; & \alpha &= \frac{\Delta m_{21}^2}{\Delta m_{31}^2}. \quad (9)
\end{aligned}$$

In presence of a_{ee} , the replacement $\hat{A} \rightarrow \hat{A}[1 + a_{ee}/\sqrt{2}G_F N_e] \simeq \hat{A} + a_{ee}/(2E/\Delta m_{31}^2)$ has to be made. In order to understand the impact of the LIV parameters, we first have a look at the oscillation probability at the P2O baseline of 2595 km. This was estimated numerically using the widely used General Long Baseline Experiment Simulator (GLOBES) [76, 77] and the associated package *snu.c* [78, 79] with necessary modifications. We consider Normal mass ordering (NO) and take the following best fit values [8] of the oscillation parameters: $\theta_{12} = 34.3^\circ, \theta_{13} = 8.58^\circ, \theta_{23} = 48.8^\circ, \delta_{13} = -0.68\pi, \Delta m_{21}^2 = 7.5 \times 10^{-5} \text{ eV}^2, \Delta m_{31}^2 = 2.5 \times 10^{-3} \text{ eV}^2$. We take one LIV parameter $a_{\alpha\beta}$ non-zero (fixed at the same numerical value of $5 \times 10^{-23} \text{ GeV}$, and the associated CP phase $\varphi_{\alpha\beta} = 0$) at a time to assess the role of individual LIV parameters in the probability level, and show the results in Fig. 1.

As expected, the appearance channel is most affected by the LIV parameters $a_{e\mu}$ and $a_{e\tau}$. Compared to the standard case (black dashed curve), $a_{e\mu}$ increases the magnitude of $P(\nu_\mu \rightarrow \nu_e)$ while the presence of $a_{e\tau}$ shows a depletion around the oscillation maxima of 4–5 GeV. This is due to the fact that both the $\sin \delta_{13}$ and $\cos \delta_{13}$ terms within the square brackets of Eq. 8 have the same sign (negative, thus decreasing $P_{\mu e}$), while there is a relative sign between two such terms in Eq. 7, - thus leading to a smaller enhancement of $P_{\mu e}$. The effects of $a_{e\mu}$ and $a_{e\tau}$ become qualitatively opposite for the $P_{\bar{\nu}_\mu \rightarrow \bar{\nu}_e}$ channel. We also observe that a_{ee} increases or decreases the probabilities only mildly. The disappearance channel, on the other hand is impacted by only the parameters $a_{\mu\mu}$ and $a_{\mu\tau}$, - the changes induced by them being in the opposite direction for ν and $\bar{\nu}$ -modes.

The sensitivity to the LIV parameters depends on the change in probability due to the presence of LIV:

$$\Delta P_{\alpha\beta} = P_{\alpha\beta}(\text{SI+LIV}) - P_{\alpha\beta}(\text{SI}), \quad (\alpha, \beta = e, \mu, \tau). \quad (10)$$

In order to have an approximate idea about the physics behind the sensitivity estimates, we focus on the dominant channel, *i.e.*, the $\nu_\mu \rightarrow \nu_e$ channel and the most relevant LIV parameters $a_{e\mu}, a_{e\tau}, a_{ee}$.

In Fig. 2 we show by means of a heatmap, how the absolute difference $|\Delta P_{\mu e}|$ evolves with variation in the LIV parameters and the variation in the standard CP phase δ_{13} , for a fixed baseline and energy. In top (bottom) row, we consider the baseline 2595 (1300) km and approximate first

oscillation maximum energy 5 (2.5) GeV for the P2O (DUNE) experiment. The light yellow end of the colour spectrum corresponds to lower $|\Delta P_{\mu e}|$ (*i.e.*, more degeneracy between SI and LIV), while the darker shades indicate a higher impact of the corresponding LIV parameter, resulting in a higher value of $|\Delta P_{\mu e}|$.

In all the heatplots we see that there is little to no change in the probability for very small values of the LIV parameter, which is consistent with our expectation. In presence of $a_{e\mu}$ ($a_{e\tau}$), we note the presence of a set of two degenerate (yellow) *branches* appearing at two different values of δ_{13} . Interestingly these degeneracies remain present irrespective of the values of $|a_{e\mu}|$ or $|a_{e\tau}|$ and the degenerate regions are almost parallel to the LIV parameter axis. These features are more prominent for the P2O baseline than the DUNE baseline. On the other hand, in presence of a_{ee} , P2O baseline shows an additional degeneracy approximately around $a_{ee} \simeq 22 \times 10^{-23}$ GeV, but curiously this is absent for DUNE.

For an analytical understanding of the various features, we use Eqs. 5, 6, 7, 8 to express $|\Delta P_{\mu e}|$

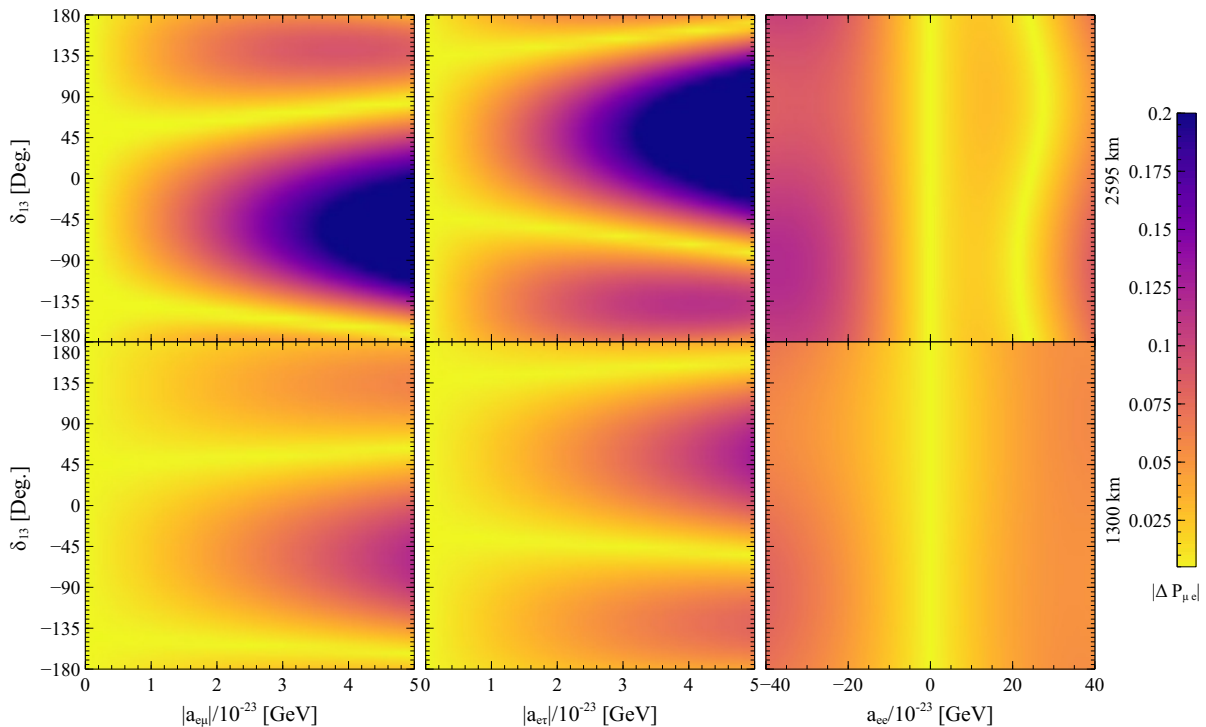


FIG. 2. We plot the heatplot for $|\Delta P_{\mu e}| = |P_{\mu e}(\text{SI+LIV}) - P_{\mu e}(\text{SI})|$ for the P2O baseline of 2595 km (top row) and for DUNE baseline of 1300 km (bottom row). The plots were done for the respective values of energies roughly corresponding to first oscillation maximum: 2.5 GeV for DUNE and 5 GeV for P2O. The heatplot is shown as a function of the three LIV parameters ($|a_{e\mu}|, |a_{e\tau}|, a_{ee}$) along the horizontal axes and the standard (Dirac) CP phase δ_{13} .

in presence of $a_{e\mu}$ or $a_{e\tau}$ as the following.

$$\Delta P_{\mu e}(|a_{e\mu}|) \simeq 8|a_{e\mu}| \frac{\pi}{2} E s_{13} \sin 2\theta_{23} c_{23} \left[-\sin \delta_{13} + \frac{2}{\pi} \frac{s_{23}^2}{c_{23}^2} \cos \delta_{13} \right], \quad (11)$$

$$\Delta P_{\mu e}(|a_{e\tau}|) \simeq 8|a_{e\tau}| \frac{\pi}{2} E s_{13} \sin 2\theta_{23} s_{23} \left[\sin \delta_{13} + \frac{2}{\pi} \cos \delta_{13} \right]. \quad (12)$$

Note that, since all the heatplots are generated corresponding to the first oscillation maximum, we put $\Delta = \Delta m_{31}^2 L/E \simeq \pi/2$ in deriving Eqs. 11 and 12. $\Delta P_{\mu e}(|a_{e\mu}|)$ (or $\Delta P_{\mu e}(|a_{e\tau}|)$) is directly proportional to $|a_{e\mu}|$ (or $|a_{e\tau}|$) respectively, - which clearly shows that for very small values of the LIV parameters, we get a degeneracy. For the pair of yellow degenerate *branches* in the first two columns of Fig. 2, the quantities inside the square brackets of Eqs. 11 and 12 need to vanish, and the solutions are independent of the value of the LIV parameter and the baseline. For the case of $|a_{e\mu}|$, this condition becomes,

$$\sin \delta_{13} = \frac{2}{\pi} \frac{s_{23}^2}{c_{23}^2} \cos \delta_{13}. \quad (13)$$

Putting $\theta_{23} = 48.8^\circ$, the solutions are $\delta_{13} \simeq 39^\circ, -141^\circ$. It is clear from the $(s_{23}/c_{23})^2$ factor that for θ_{23} lying in the higher octant, first solution for δ_{13} will move (mildly) closer to $\pi/4$, making the second solution move towards $-3\pi/4$. For the case of $|a_{e\tau}|$, using Eq. 12 the degenerate condition translates to,

$$\sin \delta_{13} = -\frac{2}{\pi} \cos \delta_{13}, \quad (14)$$

the solutions of which are given by roughly $\delta_{13} \simeq -33^\circ, 147^\circ$. We note that the solutions for δ_{13} for Eqs. 13 and 14 for the locations of degeneracies approximately differ by a sign (as long as θ_{23} does not lie too far from the maximal value of $\pi/4$), or equivalently they differ by a $\pm\pi/2$ phase-shift. These locations of degeneracies and the shift of the solutions for $|a_{e\mu}|$ and $|a_{e\tau}|$ are consistent with Fig. 2. The slight *slanting* nature of the degenerate branches with increase in $|a_{e\mu}|$ originates due to subdominant higher order terms, which we have not considered in our simplified analysis. In Fig. 2, we note that deviation from the standard case happens more quickly when the CP phase $\delta_{13} \in [-\pi/2, 0]$ (for $|a_{e\mu}|$) and $\delta_{13} \in [0, \pi/2]$ (for $|a_{e\tau}|$), - manifested by the presence of darker patches around $|a_{e\mu}|$ or $|a_{e\tau}| \gtrsim 2 \times 10^{-23}$ GeV. These two separate quadrants for δ_{13} originate due to the presence of the relative sign between the $\sin \delta_{13}$ and $\cos \delta_{13}$ terms inside the square brackets in Eqs. 11 and 12. The proportionality of Eqs. 11 and 12 with energy suggests that the features are quantitatively more prominent for P2O than DUNE, since the peak energy corresponding to the former is twice the latter (5 GeV, as compared to 2.5 GeV for DUNE). To understand the features

induced by the presence of a_{ee} , we deduce the corresponding probability difference as follows (using Eq. 6 and replacing $\hat{A} \rightarrow \hat{A}[1 + a_{ee}/\sqrt{2}G_F N_e]$ to account for a_{ee}).

$$\Delta P_{\mu e}(a_{ee}) \simeq 4s_{13}^2 c_{13}^2 s_{23}^2 \left\{ \frac{\sin^2 [1 - \hat{A}(1 + a_{ee}/\sqrt{2}G_F N_e)] \Delta}{[1 - \hat{A}(1 + a_{ee}/\sqrt{2}G_F N_e)]^2} - \frac{\sin^2 [1 - \hat{A}] \Delta}{[1 - \hat{A}]^2} \right\} + \cos \delta_{13}\text{-term.} \quad (15)$$

The $\cos \delta_{13}$ -term containing Y from Eq. 6 is suppressed by a factor α ($= \Delta m_{21}^2 / \Delta m_{31}^2 \sim 10^{-2}$) compared to the first term in Eq. 15. We neglect this term for simplicity. Thus the degeneracy condition ($\Delta P_{\mu e}(a_{ee}) \simeq 0$) in presence of a_{ee} can be simplified to the following equation.

$$\underbrace{\left[\frac{\sin [1 - \hat{A}(1 + \hat{a}_{ee})] \Delta}{1 - \hat{A}(1 + \hat{a}_{ee})} - \frac{\sin [1 - \hat{A}] \Delta}{1 - \hat{A}} \right]}_{I_-} \times \underbrace{\left[\frac{\sin [1 - \hat{A}(1 + \hat{a}_{ee})] \Delta}{1 - \hat{A}(1 + \hat{a}_{ee})} + \frac{\sin [1 - \hat{A}] \Delta}{1 - \hat{A}} \right]}_{I_+} = 0, \quad (16)$$

where $\hat{a}_{ee} = a_{ee}/\sqrt{2}G_F N_e$. It is easy to see that I_+ cannot be zero, and for I_- to vanish we

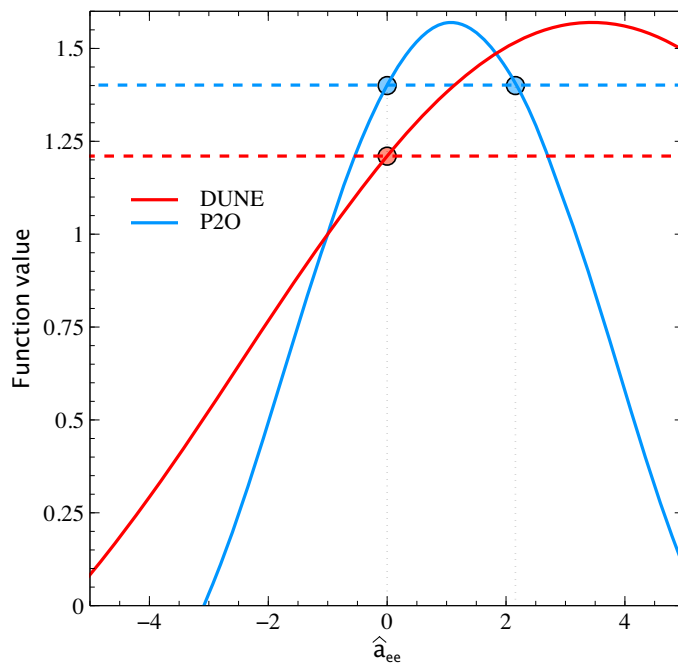


FIG. 3. The two terms in I_- from Eq. 16 are plotted for both DUNE (red) and P2O (blue) as functions of the parameter $\hat{a}_{ee} = a_{ee}/\sqrt{2}G_F N_e$. The solid curve is the first term ($\frac{\sin[1 - \hat{A}(1 + \hat{a}_{ee})]\Delta}{1 - \hat{A}(1 + \hat{a}_{ee})}$), while the dashed curve is the second term ($\frac{\sin[1 - \hat{A}]\Delta}{1 - \hat{A}}$). The small coloured circles show the locations of solutions where the two terms intersect.

can immediately identify $a_{ee} = 0$ as the trivial solution. To examine the possibility of further

degeneracies, we note the following.

$$\Delta \simeq \pi/2; \quad (\text{for both P2O and DUNE})$$

$$\hat{A} \simeq \frac{2\sqrt{2}G_F N_e E}{\Delta m_{31}^2} \simeq 0.03 \times \rho[\text{g}\cdot\text{cm}^{-3}] \times E[\text{GeV}] \simeq \begin{cases} 0.225, & (\text{for DUNE}, \rho \simeq 3, E \simeq 2.5) \\ 0.448. & (\text{for P2O}, \rho \simeq 3.2, E \simeq 5). \end{cases} \quad (17)$$

To find other solutions when $I_- = 0$, we plot the two terms in I_- for both DUNE and P2O as a function of the parameter \hat{a}_{ee} in Fig. 3. The first term is an oscillating function of \hat{a}_{ee} , while

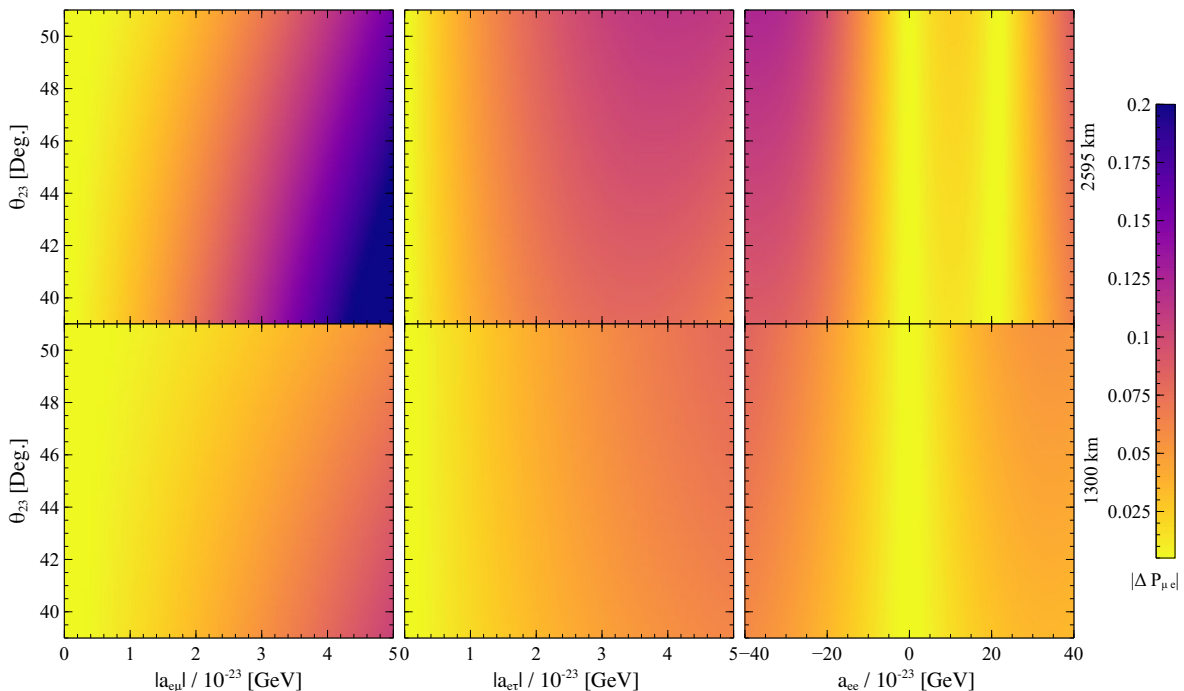


FIG. 4. Similar to Fig. 2 but shown as a function of θ_{23} with fixed δ_{13} .

the second term is a constant. For DUNE, having a lower baseline and energy, the *sine* function (red solid) oscillates slowly and has only the trivial solution in the range shown. Corresponding *sine* function for P2O (blue solid) oscillates faster, given the larger baseline and energy, and thus can have a second (non-trivial) solution at a reasonably smaller positive value of $\hat{a}_{ee} \simeq 2.2$, which translates to $a_{ee} = 2.2\sqrt{2}G_F N_e \simeq 24.8 \times 10^{-23}$ GeV. This is almost exactly the location of the second degeneracy in the top right panel of Fig. 2. The mild dependence of this degeneracy branch on the CP phase δ_{13} arises from the $\cos \delta_{13}$ -term in Eq. 15 which we have neglected for simplicity.

In Fig. 4, we show the heatplot for $|\Delta P_{\mu e}|$ in the parameter space of θ_{23} and one LIV parameter ($|a_{e\mu}|, |a_{e\tau}|, a_{ee}$), for a fixed CP phase $\delta_{13} = -0.68\pi$. Comparing the first and the middle columns,

we see that $a_{e\mu}$ has a slightly bigger impact than $a_{e\tau}$. Moreover, presence of $a_{e\mu}$ induces more deviation at lower octant (LO), while that of $a_{e\tau}$ is apparent at higher octant (HO). If we look at the analytical expressions for $\Delta P_{\mu e}$ in Eqs. 11 and 12, this octant dependence originates due to the overall factor c_{23} in presence of $a_{e\mu}$ and s_{23} in presence of $a_{e\tau}$ (note that the factor $\sin 2\theta_{23}$ in those equations are octant-independent). In the third column of Fig. 4, a_{ee} again gives rise to additional degeneracy for P2O, which has already been explained above with regard to Fig. 2.

IV. SIMULATION DETAILS

We simulate the long baseline neutrino experiments DUNE and P2O using GLoBES [76, 77] and use the add-on *snu.c* [78, 79] to implement the physics of LIV. DUNE is a 1300 km long baseline experiment from the accelerator at the site of FermiLab to the site employing a liquid argon far detector (FD) of 40 kt fiducial mass at South Dakota. The experiment is capable of using a proton beam of power 1.07 MW and of running 3.5 years each on ν and $\bar{\nu}$ mode (resulting in a total exposure of roughly 300 kt.MW.yr corresponding to total 1.47×10^{21} protons on target or POT). The flux, cross-sections, migration matrices for energy reconstruction, efficiencies *etc.* were implemented according to the official configuration files [80] provided by the DUNE collaboration for its simulation.

P2O (Protvino to ORCA) is a proposed long baseline neutrino experiment with a baseline of nearly 2595 km from the Protvino accelerator complex, situated at 100 km south of Moscow to the site of ORCA (Oscillation Research with Cosmics in the Abyss), hosting 6 MT Cerenkov detector located 40 km off the coast in South France, at a mooring depth of 2450 m in the Mediterranean sea. ORCA is the low energy component of the KM3NeT Consortium [81], with a primary goal of studying atmospheric neutrino oscillations in the energy range of 3 to 100 GeV in order to determine the neutrino mass ordering. We simulate the nominal configuration³ of P2O experiment using a 90 kW proton beam with a runtime of 3 yrs. in ν and 3 yrs. in $\bar{\nu}$ mode, - corresponding to a total POT of 4.8×10^{20} . The fluxes, detector response parameters, the detection efficiencies, signal and background systematics *etc.*, corresponding to our nominal P2O configuration were taken from [18, 81].

To estimate the sensitivity of LBL experiments to probe the LIV parameters, we carry out a

³ There are proposals for using an upgraded proton beam with 450 kW power and also to use the Super-ORCA detector with denser geometry, lower energy thresholds and better flavour identification capabilities [18].

$\Delta\chi^2$ analysis using GLoBES. The analytical⁴ form of the $\Delta\chi^2$ can be expressed as,

$$\Delta\chi^2(p^{\text{true}}) = \text{Min}_{p^{\text{test}}, \eta} \left[2 \sum_k^{\text{mode}} \sum_j^{\text{channel}} \sum_i^{\text{bin}} \left\{ N_{ijk}^{\text{test}}(p^{\text{test}}; \eta) - N_{ijk}^{\text{true}}(p^{\text{true}}) + N_{ijk}^{\text{true}}(p^{\text{true}}) \ln \frac{N_{ijk}^{\text{true}}(p^{\text{true}})}{N_{ijk}^{\text{test}}(p^{\text{test}}; \eta)} \right\} + \sum_l \frac{(p_l^{\text{true}} - p_l^{\text{test}})^2}{\sigma_{p_l}^2} + \sum_m \frac{\eta_m^2}{\sigma_{\eta_m}^2} \right]. \quad (18)$$

N^{true} corresponds to the simulated set of event spectra corresponding to *true* set of oscillation parameters p^{true} , while N^{test} denotes the events simulated in presence of LIV (the set of relevant parameters being p^{test}). The sums over the three indices i, j, k signify the summations over the energy bins, the oscillation channels (ν_e appearance and ν_μ disappearance), and the running modes (neutrino and antineutrino modes) respectively. For DUNE we take a total 71 energy bins in the range of 0 – 20 GeV, - with 64 bins with uniform width of 0.125 GeV in the energy range of 0 to 8 GeV and 7 bins with varying widths beyond 8 GeV [80]. Thus the first term ($N^{\text{test}} - N^{\text{true}}$) inside the curly braces accounts for the algebraic difference between the two sets of data, whereas the log-term gives a kind of fractional difference between them. The entire expression in the curly brackets with summations over i, j, k consists of the statistical part of the $\Delta\chi^2$.

Uncertainties in the prior measurement of the l^{th} oscillation parameter are given by the parameters σ_{p_l} . η_m is the nuisance parameter/systematics and σ_{η_m} is the corresponding uncertainty. For DUNE, the ν_e and $\bar{\nu}_e$ signal modes have a normalization uncertainties of 2% each, whereas the ν_μ and $\bar{\nu}_\mu$ signals have a normalization uncertainty of 5% each. For P2O, these numbers were taken as 5% for all the four types of signals. The background normalization uncertainties vary within 5% – 20% (for DUNE) and 10% – 15% (for P2O), and include correlations among various sources of backgrounds (contamination of $\nu_e/\bar{\nu}_e$ in the incident beam, flavour misidentification, neutral current and ν_τ). The term summed over l takes care of the precision measurements in the oscillation parameters and the last term (summed over m) is the systematics part. This way of treating the systematics in the $\Delta\chi^2$ calculation is known as the *method of pulls* [82–85].

For the true set oscillation parameters we use the bestfit values from [8], as mentioned in Sec. III. The final estimate of the (minimum) $\Delta\chi^2$ obtained after a marginalization over the 3σ range of test parameters [8] and the set of systematics (η) is a function of the true values of the oscillation parameters. We marginalize over the standard oscillation parameters θ_{23} , δ_{13} , Δm_{31}^2 (both the magnitude and sign) and also the LIV CP phases $\varphi_{\alpha\beta}$ wherever applicable. The $\Delta\chi^2$ thus estimated is the frequentist method of hypotheses testing [83, 86].

⁴ This is the *Poissonian* definition of $\Delta\chi^2$, which in the limit of large sample size, reduces to the Gaussian form.

V. CORRELATIONS AMONG THE LIV PARAMETERS

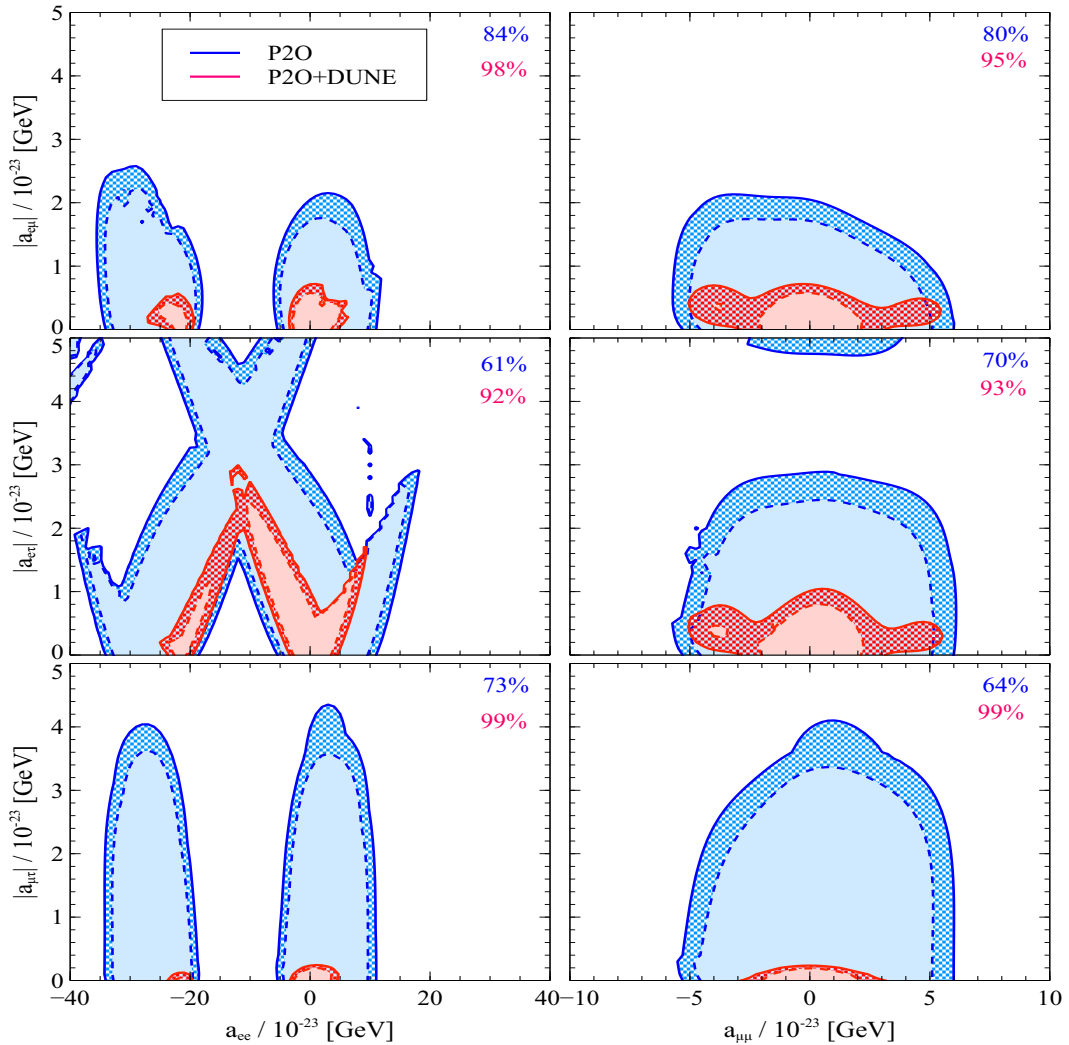


FIG. 5. This shows the exclusion regions in the parameter space consisted of one diagonal (along the horizontal axis) and one off-diagonal LIV parameter (vertical axis) for P2O only (blue contours) and P2O combined with DUNE (red contours). The results are shown at the confidence level (C.L.) of 95% (dashed contours) and 99% (solid contours). The pair of numbers (%) in each panel indicates the area lying outside the solid (99% C.L.) contours, expressed as a percentage of the total area of the parameter space considered. The numbers are shown for the two cases, - blue for P2O only and red for the combined case of (P2O + DUNE), and thus they offer a measure of the degree of improvement of the latter over the former for each relevant parameter space.

In Fig. 5, we show the 95% (dashed contour) and 99% (solid contours) confidence level (C.L.) regions in the parameters space spanned by one off-diagonal LIV parameter $|a_{\alpha\beta}|$ ($|a_{e\mu}|$, $|a_{e\tau}|$ or $|a_{\mu\tau}|$) and one diagonal LIV parameter $a_{\alpha'\beta'}$ (a_{ee} or $a_{\mu\mu}$). The associated LIV phases ($\varphi_{e\mu}$, $\varphi_{e\tau}$ or $\varphi_{\mu\tau}$) were marginalised in the full range of $[-\pi, \pi]$ in the fit. The blue contours show the sensitivity

reach of P2O alone while the red ones illustrate the results of combining the projected data of P2O and DUNE (P2O + DUNE). For each of these two combinations, namely P2O and (P2O+DUNE), in each panel we estimate the regions excluded at 99% C.L. contours (*i.e.*, the area outside the contours with solid blue and solid red boundaries respectively), and express that as a percentage of the total area of the parameter space shown. The two numbers thus give us a quantitative measure of the improvement of the combination (P2O + DUNE) over P2O only in excluding the relevant parameter space at 99% C.L.⁵ The improvement is remarkable in all cases, covering more than 90% of the parameter space considered. In presence of a_{ee} , we observe the additional/fake degenerate region around $a_{ee} \simeq -22 \times 10^{-23}$ GeV, which arises due to marginalization over the opposite mass hierarchy. Note that the location of this fake solution is approximately opposite in sign to the degeneracies in the corresponding probability heatplots (Figs. 2 and 4: third column, top row), where the additional degeneracies were found around $a_{ee} \simeq 22 \times 10^{-23}$. It can be qualitatively understood as follows. Without considering flux and cross-sections for simplicity, the dominant statistical contribution to the sensitivity in the LIV scenario (*test* scenario) involving the parameter a_{ee} and another parameter, say c , roughly follows the corresponding probability deviation from the *true* standard case (in the similar spirit as discussion in Sec. III):

$$\Delta\chi^2(a_{ee}, c) \sim \Delta P_{\mu e}(a_{ee}) + \Delta P_{\mu e}(c) + (\text{other terms}), \quad (19)$$

where the other terms contain contributions from the $\nu_\mu \rightarrow \nu_\mu$ disappearance channel, antineutrinos, priors and systematics, - which we have neglected in order to have a simple qualitative understanding. Using our previous discussion concerning Eqs. 15 and 16, we can write,

$$\begin{aligned} \Delta\chi^2(a_{ee}, c) &\sim \Delta P_{\mu e}(a_{ee}) \\ &\sim \underbrace{\left[\frac{\sin [1 - \hat{A}(1 + \hat{a}_{ee})]\Delta}{1 - \hat{A}(1 + \hat{a}_{ee})} - \frac{\sin [1 - \hat{A}]\Delta}{1 - \hat{A}} \right]}_{I_-} \times \underbrace{\left[\frac{\sin [1 - \hat{A}(1 + \hat{a}_{ee})]\Delta}{1 - \hat{A}(1 + \hat{a}_{ee})} + \frac{\sin [1 - \hat{A}]\Delta}{1 - \hat{A}} \right]}_{I_+}. \end{aligned} \quad (20)$$

Within the same mass hierarchy for the true and test scenario, the minimum for $\Delta\chi^2(a_{ee}, c)$ is obtained at the true solution $a_{ee} \simeq 0$, making I_- vanish. But while marginalizing over the opposite mass hierarchy in the test scenario, \hat{A} and Δ changes sign in the terms containing a_{ee} , and we

⁵ Similar estimates were used in reference [75] in order to quantify the improvement of one experimental configuration over another in the context of Nonstandard neutrino interaction.

have,

$$\Delta\chi^2(a_{ee}, c) \sim \underbrace{\left[\frac{\sin [1 + \hat{A}(1 + \hat{a}_{ee})]\Delta}{1 + \hat{A}(1 + \hat{a}_{ee})} + \frac{\sin [1 - \hat{A}]\Delta}{1 - \hat{A}} \right]}_{I_-} \times \underbrace{\left[\frac{\sin [1 + \hat{A}(1 + \hat{a}_{ee})]\Delta}{1 + \hat{A}(1 + \hat{a}_{ee})} - \frac{\sin [1 - \hat{A}]\Delta}{1 - \hat{A}} \right]}_{I_+}. \quad (21)$$

Because of the relative changes of signs, now I_- cannot vanish and the minimum solution is obtained when I_+ goes to zero instead. That is obtained when $\hat{a}_{ee} = -2$ and thus $a_{ee} \simeq -22 \times 10^{-23}$ GeV. Such a degeneracy was also observed in previous analyses with LIV in case of DUNE [41]. Although a combination with DUNE significantly constrains this additional degeneracy, it still does not go away completely. For the parameter $a_{\mu\mu}$ we see the contours are roughly symmetric around the true solution $a_{\mu\mu} = 0$. If $a_{\mu\tau}$ is present, a combination with DUNE can probe almost the entire parameter space considered at a C.L. of 99%. This sensitivity to $|a_{\mu\tau}|$ mainly comes from the $\nu_\mu \rightarrow \nu_\mu$ disappearance channel.

Fig. 6 shows the $\Delta\chi^2$ correlation among the off-diagonal LIV parameters themselves ($a_{e\mu}, a_{e\tau}, a_{\mu\tau}$) and also between the two diagonal parameters a_{ee} and $a_{\mu\mu}$, for both P2O and combined (P2O+DUNE). The improvement by the combined analysis is especially prominent for the most impactful parameter space $a_{e\mu} - a_{e\tau}$ (top left panel of Fig. 6). At a C.L. of 99%, (P2O+DUNE) combination can exclude 92% of the parameter ranges considered, compared to 53% by P2O alone.

VI. DEGENERACIES WITH THE STANDARD OSCILLATION PARAMETERS

In Fig. 7 (and Fig. 8), we demonstrate how efficiently the projected data from P2O and DUNE can reconstruct the standard CP phase δ_{13} (and mixing angle θ_{23}), in correlation with the LIV parameters present. The true value of θ_{23} was taken as 48.8° and in the test dataset the marginalization was done on $\theta_{23}, \delta_{13}, \Delta m_{31}^2$ (both magnitude and the sign), as well as the LIV CP phases wherever present. At the C.L.s of 99% and 95%, the presence of all LIV parameters at P2O can give rise to allowed regions covering almost the entire δ_{13} -space. But the combination (P2O + DUNE) significantly shrinks the allowed regions to lie around the true solution of $\delta_{13} = -0.68\pi$. Similar observation holds in Fig. 8 for the parameter space containing θ_{23} also. Concerning the combined analysis of (P2O+DUNE) (*i.e.*, the solid and shaded red contours in Fig. 8), although the maximal mixing ($\theta_{23} = 45^\circ$) got excluded in case of all the LIV parameters, in case of $a_{e\mu}$ and $a_{e\tau}$ (bottom row, first and second columns of Fig. 8) we note that the allowed regions still appear in the opposite (lower) octant. We refer the readers to [43] for a more in-depth discussion regarding

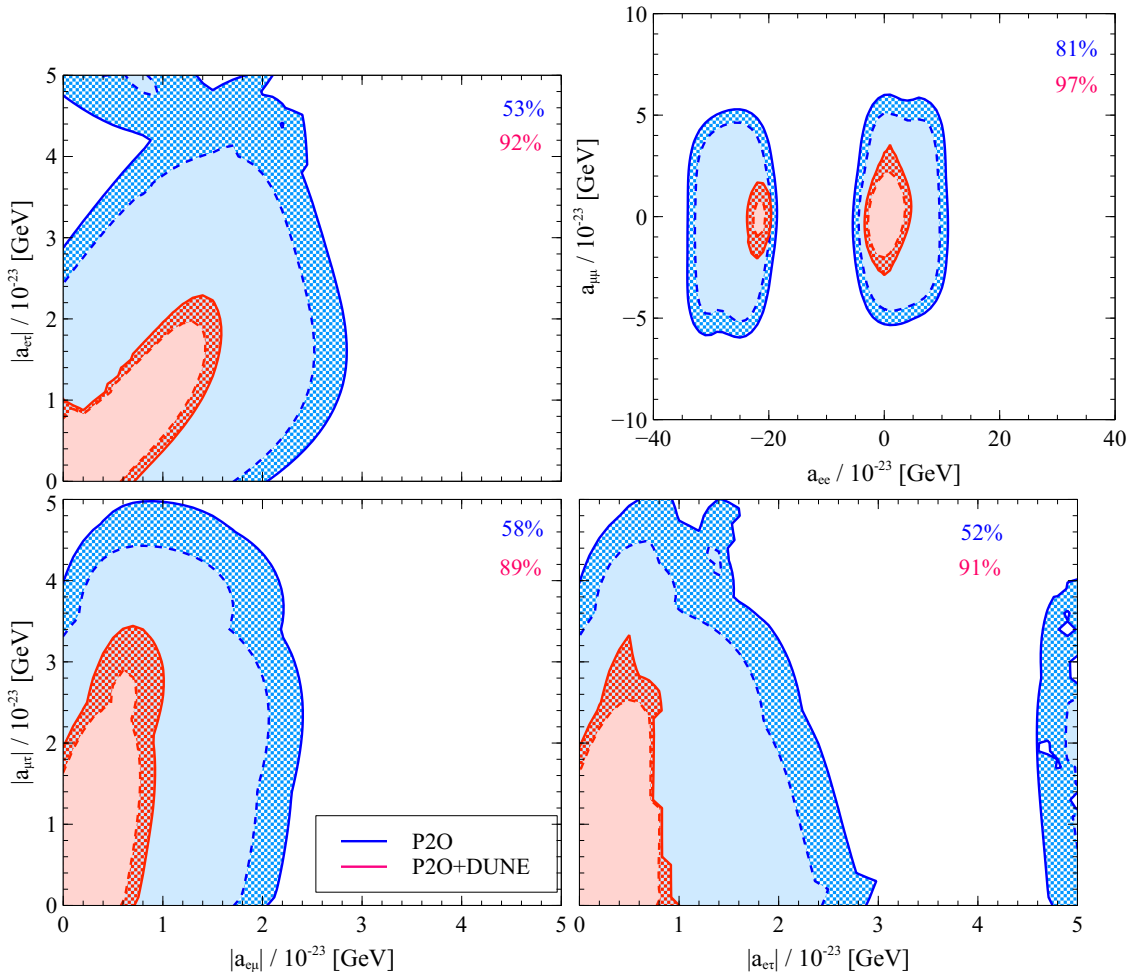


FIG. 6. Similar to Fig. 5 but shows the exclusion regions in the parameter spaces with both off-diagonal LIV parameters (left and bottom) and both diagonal LIV parameters (top right panel). The solid (dashed) contours indicate 99% and 95% C.L. regions.

the impacts of $a_{e\mu}$ and $a_{e\tau}$ on θ_{23} -octant. It is clear that for P2O alone, the exclusion region in presence of $a_{e\mu}$ is greater than in presence of $a_{e\tau}$ (60% versus 40% of the total parameter space considered, at 99% C.L.). This can be connected to the higher impact of $a_{e\mu}$ in the probability deviation $|\Delta P_{\mu e}|$ in Fig. 4 (top row, first and second column) and related discussions in Sec. III. a_{ee} generates the additional degeneracy around -22×10^{-23} GeV as usual.

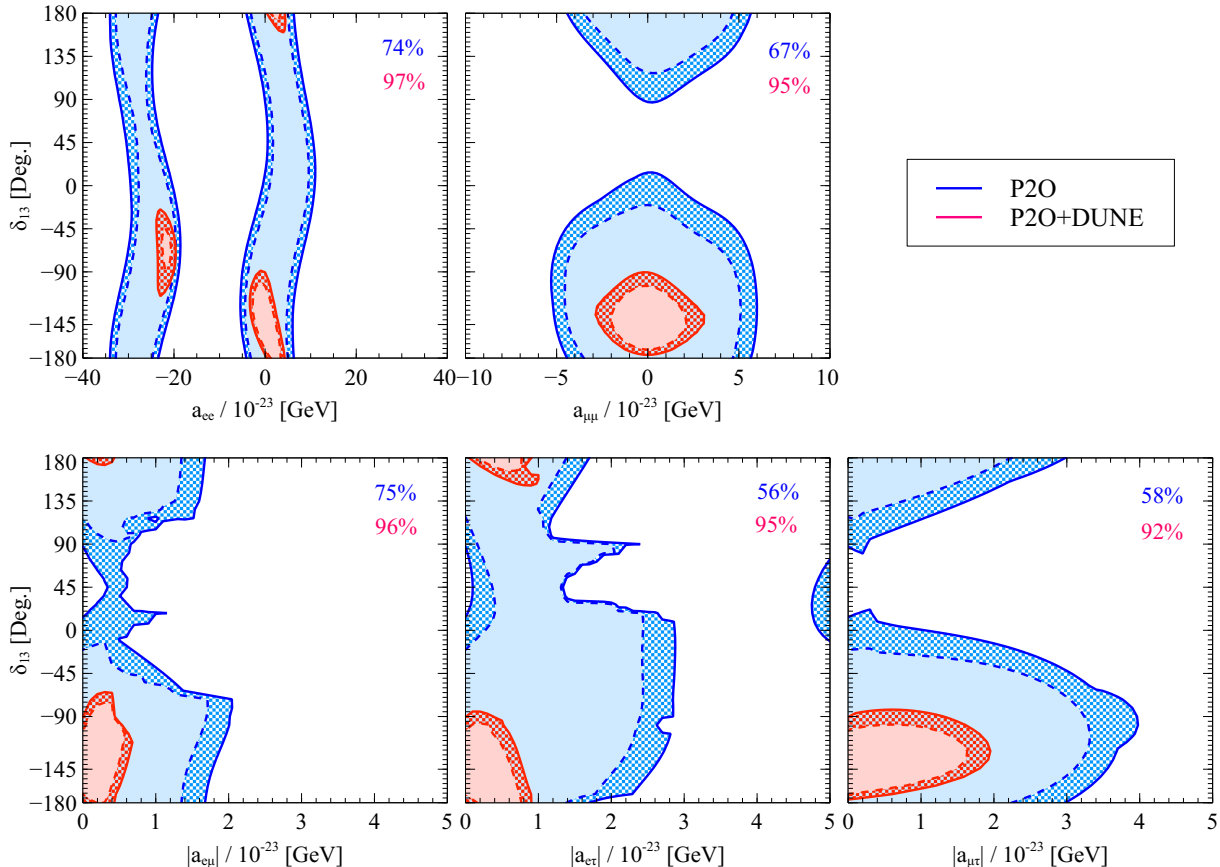


FIG. 7. Exclusion/allowed regions at 99% C.L. (solid) and 95% C.L. (dashed) showing the correlations of the LIV parameters with the CP phase δ_{CP} for P2O (blue contours) and P2O+DUNE (red contours). Similar to Fig. 5

VII. BOUNDS ON THE LIV PARAMETERS

Fig. 9 shows the one dimensional projection (after marginalising away all other parameters including the CP phases, θ_{23} , Δm_{31}^2) of $\Delta\chi^2$ as a function of each LIV parameter individually. The results are illustrated for P2O alone (blue) and for the combined analysis of (P2O + DUNE) (red) and the $\Delta\chi^2$ values corresponding to 95% and 99% C.L.s are marked with horizontal black lines. The significant increase in the steepness of the red sensitivity curves is indicative of the crucial impact of the combined analysis in constraining the LIV parameters. For a_{ee} , we note the lifting of the troublesome degeneracy at $a_{ee} \simeq -22 \times 10^{-23}$ GeV by the combined analysis above 95% C.L. This was not possible with the analysis done with DUNE alone [41] or with P2O alone. Table I shows our final result: the constraints obtained on the five LIV parameters at 95% C.L. with the combined (P2O+DUNE) analysis and compares the numbers obtained from a previous analysis [41] of DUNE alone. We note that the constraints on the diagonal parameters can be

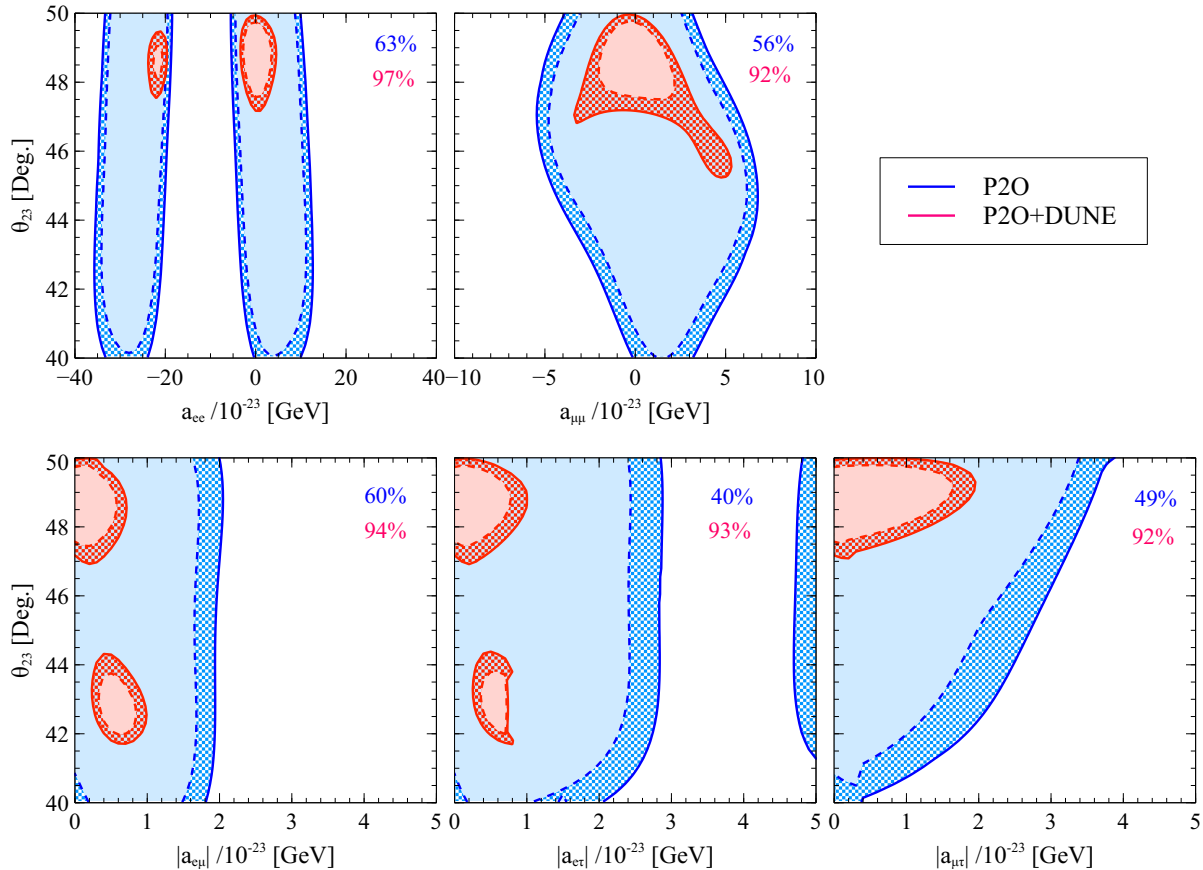


FIG. 8. Similar to Fig. 7 but showing the correlation of the LIV parameters with θ_{23} .

tightened significantly with the combined analysis. This is especially noticeable for a_{ee} since the fake solution can be ruled out at 95% C.L. as mentioned before. For $|a_{e\mu}|$, $|a_{e\tau}|$ and $|a_{\mu\tau}|$ also the bounds improve moderately.

VIII. SUMMARY AND CONCLUSION

In this work we consider the proposed long baseline experiment P2O with a 2595 km baseline from the already existing accelerator complex at Protvino to the far detector situated at the site of ORCA/KM3NET with a fiducial mass of approximately 6 Mt. and a peak energy of around 4-5 GeV. Such a long baseline offers very high sensitivity to neutrino mass hierarchy and the massive far detector provides very high statistics even with a relatively moderate 90 kW proton beam. In this work, we have discussed the capability of an LBL experiment to probe fundamental theories of quantum gravity that can potentially manifest itself in the form of Lorentz Invariance Violation (LIV) around this energy range. We first discuss how the probabilities can deviate from

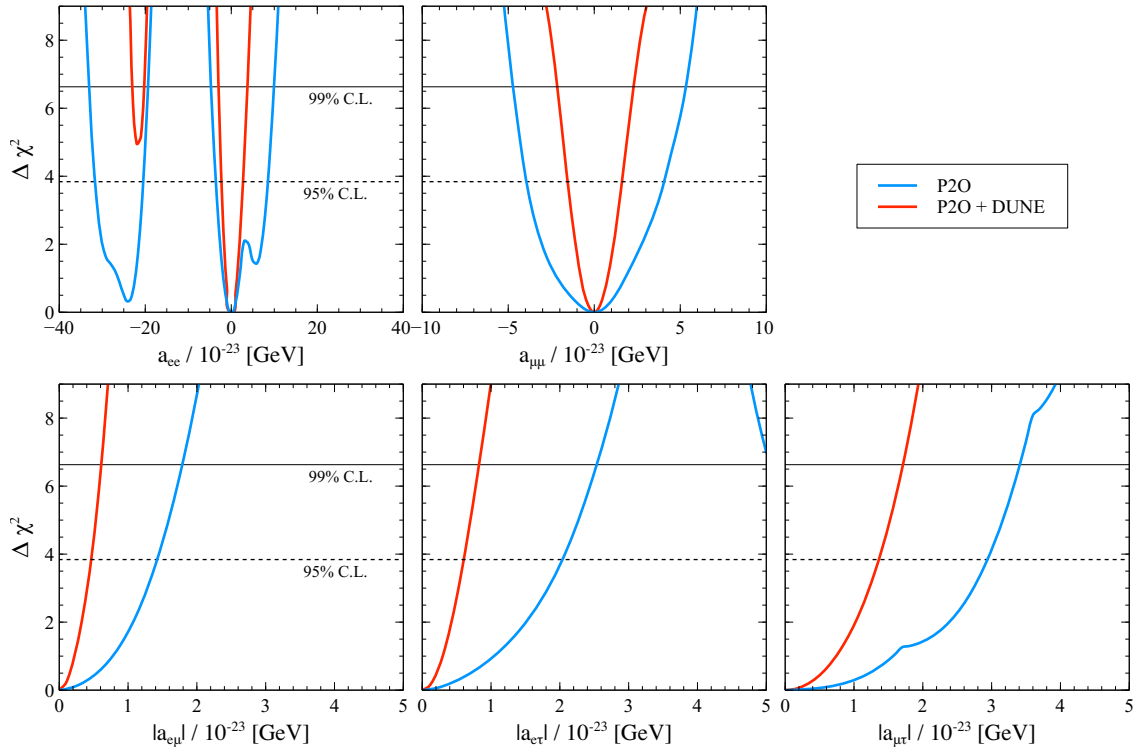


FIG. 9. Expected sensitivity of P2O (blue) and the combined (P2O+DUNE) (red) analysis to the LIV parameters. The black dotted (solid) line indicates the 95% (99%) C.L. at 1 degree of freedom. Each panel corresponds to individual LIV parameter.

the standard interaction (SI) scenario by different Lorentz violating parameters (which are also CPT-violating) at the P2O baseline. We then analytically derive the approximate changes in the appearance probabilities, $\Delta P_{\mu e} (= P_{\mu e}(\text{SI+LIV}) - P_{\mu e}(\text{SI}))$ that are induced by individual LIV parameters. We illustrate by means of heatplots of $\Delta P_{\mu e}$, how the LIV parameters impact at the baseline of P2O at its peak energy and compare it with DUNE experiment. In presence of $a_{e\mu}$ and $a_{e\tau}$, we find interesting degenerate branches (existing even for larger values of the LIV parameters) at specific values of the standard CP phase δ_{13} . As a function of θ_{23} , we observe that the impact of $a_{e\mu}$ on $\Delta P_{\mu e}$ is slightly higher than that of $a_{e\tau}$. These features were also explained with the help of probability expressions in presence of these two parameters. We also find two degenerate regions at the level of probability for $a_{ee} \simeq 0, 22 \times 10^{-23}$ GeV, whereas for DUNE we find only the trivial one at $a_{ee} = 0$. We explain this by breaking down the corresponding $\Delta P_{\mu e}$ and showing that the relevant *sine*-term oscillates faster for P2O (due to higher peak energy and a slightly higher value of average baseline density), - forcing a second nontrivial solution. We then proceed to estimate $\Delta\chi^2$ sensitivities to LIV parameters for P2O alone and also discuss how significantly the

Parameter	Existing bounds ($\times 10^{-23}$) [GeV] [41] (from DUNE)	Bounds from this work ($\times 10^{-23}$) [GeV] (P2O+DUNE)
a_{ee}	$[-25 < a_{ee} < -20] \cup [-2.5 < a_{ee} < 3.2]$	$-2.093 < a_{ee} < 2.728$
$a_{\mu\mu}$	$-3.7 < a_{\mu\mu} < 4.8$	$-1.504 < a_{\mu\mu} < 1.660$
$ a_{e\mu} $	0.7	0.467
$ a_{e\tau} $	1.0	0.599
$ a_{\mu\tau} $	1.7	1.370

TABLE I. Bounds on the LIV parameters as obtained from the LBL data (P2O and DUNE combined) at 95% C.L. in comparison to the bounds shown in [41].

results improve when the simulated data of P2O is combined with that of DUNE. The sensitivity analyses were carried out by showing correlations of the LIV parameters ($a_{ee}, a_{\mu\mu}, a_{e\mu}, a_{e\tau}, a_{\mu\tau}$) among themselves and also with the two standard oscillation parameters δ_{13} and θ_{23} . For a_{ee} we discuss in detail analytically how a crucial change in sign due to marginalization over the opposite mass hierarchy produces a *fake* $\Delta\chi^2$ minimum around $a_{ee} \simeq -22 \times 10^{-23}$ GeV. For all the parameter spaces we numerically estimate the area of the regions that are excluded (at 99% C.L.) by P2O alone and compare it to that by the combined analysis of (P2O + DUNE). The significance quantitative increase in the excluded area for (P2O+DUNE) shows the overwhelming advantage of the combined analysis in all cases. Finally we calculate the one-dimensional $\Delta\chi^2$ projections as a function of all five individual LIV parameters after marginalisation over all other parameters and estimate the 95% C.L. constraints. On comparison with similar analyses done using DUNE alone, we find that for the diagonal LIV parameters there is a significant improvement of the constraints estimated in this work with the combined (P2O+DUNE) analysis. Especially noteworthy is the lifting of degeneracy around $a_{ee} \simeq -22 \times 10^{-23}$ GeV, which was earlier not possible with DUNE-only analysis. For the off-diagonal LIV parameters also our estimated bounds improve moderately upon the existing ones.

ACKNOWLEDGEMENT

MM acknowledges the support from IBS under the project code IBS-R018-D1. We thank D. Zabarov for providing us with the P2O flux files. NRKC gratefully acknowledges the financial

support of the Ministry of Science, Innovation and Universities: State Program of Generation of Knowledge, ref. PGC2018-096663-B-C41 (MCIU / FEDER), Spain.

-
- [1] SUPER-KAMIOKANDE COLLABORATION collaboration, *Evidence for oscillation of atmospheric neutrinos*, *Phys.Rev.Lett.* **81** (1998) 1562 [[hep-ex/9807003](#)].
- [2] SNO collaboration, *Direct evidence for neutrino flavor transformation from neutral current interactions in the Sudbury Neutrino Observatory*, *Phys. Rev. Lett.* **89** (2002) 011301 [[nucl-ex/0204008](#)].
- [3] A. Sakharov, *Violation of CP Invariance, C asymmetry, and baryon asymmetry of the universe*, *Sov. Phys. Usp.* **34** (1991) 392.
- [4] T2K collaboration, *Observation of Electron Neutrino Appearance in a Muon Neutrino Beam*, *Phys. Rev. Lett.* **112** (2014) 061802 [[1311.4750](#)].
- [5] NOvA collaboration, *NOvA: Proposal to Build a 30 Kiloton Off-Axis Detector to Study $\nu_\mu \rightarrow \nu_e$ Oscillations in the NuMI Beamline*, [hep-ex/0503053](#).
- [6] T2K collaboration, *Constraint on the matter–antimatter symmetry-violating phase in neutrino oscillations*, *Nature* **580** (2020) 339 [[1910.03887](#)].
- [7] NOvA collaboration, *First Measurement of Neutrino Oscillation Parameters using Neutrinos and Antineutrinos by NOvA*, *Phys. Rev. Lett.* **123** (2019) 151803 [[1906.04907](#)].
- [8] P. de Salas, D. Forero, S. Gariazzo, P. Martínez-Miravé, O. Mena, C. Ternes et al., *2020 Global reassessment of the neutrino oscillation picture*, [2006.11237](#).
- [9] Valencia-Globalfit. <http://globalfit.astroparticles.es/>, 2020.
- [10] F. Capozzi, E. Di Valentino, E. Lisi, A. Marrone, A. Melchiorri and A. Palazzo, *Global constraints on absolute neutrino masses and their ordering*, *Phys. Rev. D* **95** (2017) 096014 [[2003.08511](#)].
- [11] I. Esteban, M. C. Gonzalez-Garcia, A. Hernandez-Cabezudo, M. Maltoni and T. Schwetz, *Global analysis of three-flavour neutrino oscillations: synergies and tensions in the determination of θ_{23} , δ_{CP} , and the mass ordering*, *JHEP* **01** (2019) 106 [[1811.05487](#)].
- [12] DUNE collaboration, *Long-Baseline Neutrino Facility (LBNF) and Deep Underground Neutrino Experiment (DUNE) Conceptual Design Report Volume 2: The Physics Program for DUNE at LBNF*, [1512.06148](#).
- [13] DUNE collaboration, *Deep Underground Neutrino Experiment (DUNE), Far Detector Technical Design Report, Volume II DUNE Physics*, [2002.03005](#).
- [14] HYPER-KAMIOKANDE PROTO-COLLABORATION collaboration, *Physics potential of a long-baseline neutrino oscillation experiment using a J-PARC neutrino beam and Hyper-Kamiokande*, *PTEP* **2015** (2015) 053C02 [[1502.05199](#)].

- [15] HYPER-KAMIOKANDE collaboration, *Physics potentials with the second Hyper-Kamiokande detector in Korea*, *PTEP* **2018** (2018) 063C01 [[1611.06118](#)].
- [16] ESSNUSB collaboration, *A very intense neutrino super beam experiment for leptonic CP violation discovery based on the European spallation source linac*, *Nucl. Phys. B* **885** (2014) 127 [[1309.7022](#)].
- [17] JUNO collaboration, *Neutrino Physics with JUNO*, *J. Phys. G* **43** (2016) 030401 [[1507.05613](#)].
- [18] A. V. Akhondinov et al., *Letter of Interest for a Neutrino Beam from Protvino to KM3NeT/ORCA*, *Eur. Phys. J. C* **79** (2019) 758 [[1902.06083](#)].
- [19] O. W. Greenberg, *CPT violation implies violation of Lorentz invariance*, *Phys. Rev. Lett.* **89** (2002) 231602 [[hep-ph/0201258](#)].
- [20] V. A. Kostelecky and S. Samuel, *Spontaneous Breaking of Lorentz Symmetry in String Theory*, *Phys. Rev.* **D39** (1989) 683.
- [21] V. A. Kostelecky and S. Samuel, *Phenomenological Gravitational Constraints on Strings and Higher Dimensional Theories*, *Phys. Rev. Lett.* **63** (1989) 224.
- [22] V. A. Kostelecky and R. Potting, *CPT and strings*, *Nucl. Phys.* **B359** (1991) 545.
- [23] V. A. Kostelecky and R. Potting, *CPT, strings, and meson factories*, *Phys. Rev.* **D51** (1995) 3923 [[hep-ph/9501341](#)].
- [24] V. A. Kostelecky and R. Potting, *Expectation values, Lorentz invariance, and CPT in the open bosonic string*, *Phys. Lett.* **B381** (1996) 89 [[hep-th/9605088](#)].
- [25] D. Colladay and V. A. Kostelecky, *CPT violation and the standard model*, *Phys. Rev.* **D55** (1997) 6760 [[hep-ph/9703464](#)].
- [26] D. Colladay and V. A. Kostelecky, *Lorentz violating extension of the standard model*, *Phys. Rev.* **D58** (1998) 116002 [[hep-ph/9809521](#)].
- [27] V. A. Kostelecky, *Gravity, Lorentz violation, and the standard model*, *Phys. Rev. D* **69** (2004) 105009 [[hep-th/0312310](#)].
- [28] LSND collaboration, *Tests of Lorentz violation in anti- $\nu(\mu)$ \rightarrow anti- $\nu(e)$ oscillations*, *Phys. Rev. D* **72** (2005) 076004 [[hep-ex/0506067](#)].
- [29] MINOS collaboration, *Testing Lorentz Invariance and CPT Conservation with NuMI Neutrinos in the MINOS Near Detector*, *Phys. Rev. Lett.* **101** (2008) 151601 [[0806.4945](#)].
- [30] MINOS collaboration, *A Search for Lorentz Invariance and CPT Violation with the MINOS Far Detector*, *Phys. Rev. Lett.* **105** (2010) 151601 [[1007.2791](#)].
- [31] MINIBOONE collaboration, *Test of Lorentz and CPT violation with Short Baseline Neutrino Oscillation Excesses*, *Phys. Lett. B* **718** (2013) 1303 [[1109.3480](#)].
- [32] DOUBLE CHOOZ collaboration, *First Test of Lorentz Violation with a Reactor-based Antineutrino Experiment*, *Phys. Rev. D* **86** (2012) 112009 [[1209.5810](#)].
- [33] SUPER-KAMIOKANDE collaboration, *Test of Lorentz invariance with atmospheric neutrinos*, *Phys. Rev. D* **91** (2015) 052003 [[1410.4267](#)].

- [34] T2K collaboration, *Search for Lorentz and CPT violation using sidereal time dependence of neutrino flavor transitions over a short baseline*, *Phys. Rev. D* **95** (2017) 111101 [1703.01361].
- [35] ICECUBE collaboration, *Neutrino Interferometry for High-Precision Tests of Lorentz Symmetry with IceCube*, *Nature Phys.* **14** (2018) 961 [1709.03434].
- [36] A. Dighe and S. Ray, *CPT violation in long baseline neutrino experiments: A Three flavor analysis*, *Phys.Rev.* **D78** (2008) 036002 [0802.0121].
- [37] G. Barenboim and J. D. Lykken, *MINOS and CPT-violating neutrinos*, *Phys. Rev.* **D80** (2009) 113008 [0908.2993].
- [38] B. Rebel and S. Mufson, *The Search for Neutrino-Antineutrino Mixing Resulting from Lorentz Invariance Violation using neutrino interactions in MINOS*, *Astropart. Phys.* **48** (2013) 78 [1301.4684].
- [39] A. de Gouvea and K. J. Kelly, *Neutrino vs. Antineutrino Oscillation Parameters at DUNE and Hyper-Kamiokande*, *Phys. Rev.* **D96** (2017) 095018 [1709.06090].
- [40] G. Barenboim, C. A. Ternes and M. Tórtola, *Neutrinos, DUNE and the world best bound on CPT violation*, [1712.01714](#).
- [41] G. Barenboim, M. Masud, C. A. Ternes and M. Tórtola, *Exploring the intrinsic Lorentz-violating parameters at DUNE*, *Phys. Lett. B* **788** (2019) 308 [1805.11094].
- [42] R. Majhi, S. Chembra and R. Mohanta, *Exploring the effect of Lorentz invariance violation with the currently running long-baseline experiments*, *Eur. Phys. J. C* **80** (2020) 364 [1907.09145].
- [43] S. Kumar Agarwalla and M. Masud, *Can Lorentz invariance violation affect the sensitivity of deep underground neutrino experiment?*, *Eur. Phys. J. C* **80** (2020) 716 [1912.13306].
- [44] U. Rahaman, *Looking for Lorentz invariance violation (LIV) in the latest long baseline accelerator neutrino oscillation data*, *Eur. Phys. J. C* **81** (2021) 792 [2103.04576].
- [45] C. Giunti and M. Laveder, *Hint of CPT Violation in Short-Baseline Electron Neutrino Disappearance*, *Phys. Rev.* **D82** (2010) 113009 [1008.4750].
- [46] A. Datta, R. Gandhi, P. Mehta and S. U. Sankar, *Atmospheric neutrinos as a probe of CPT and Lorentz violation*, *Phys. Lett.* **B597** (2004) 356 [hep-ph/0312027].
- [47] A. Chatterjee, R. Gandhi and J. Singh, *Probing Lorentz and CPT Violation in a Magnetized Iron Detector using Atmospheric Neutrinos*, *JHEP* **1406** (2014) 045 [1402.6265].
- [48] B. Singh Koranga and P. Khurana, *CPT Violation in Atmospheric Neutrino Oscillation: A Two Flavour Matter Effects*, *Int. J. Theor. Phys.* **53** (2014) 3737.
- [49] S. Sahoo, A. Kumar and S. K. Agarwalla, *Probing Lorentz Invariance Violation with atmospheric neutrinos at INO-ICAL*, *JHEP* **03** (2022) 050 [2110.13207].
- [50] J. S. Diaz and T. Schwetz, *Limits on CPT violation from solar neutrinos*, *Phys. Rev.* **D93** (2016) 093004 [1603.04468].
- [51] D. Hooper, D. Morgan and E. Winstanley, *Lorentz and CPT invariance violation in high-energy neutrinos*, *Phys. Rev.* **D72** (2005) 065009 [hep-ph/0506091].

- [52] G. Tomar, S. Mohanty and S. Pakvasa, *Lorentz Invariance Violation and IceCube Neutrino Events*, *JHEP* **11** (2015) 022 [1507.03193].
- [53] J. Liao and D. Marfatia, *IceCube's astrophysical neutrino energy spectrum from CPT violation*, *Phys. Rev.* **D97** (2018) 041302 [1711.09266].
- [54] V. A. Kostelecky and N. Russell, *Data Tables for Lorentz and CPT Violation*, 0801.0287.
- [55] D. Zaborov, "Scientific Potential of a neutrino beam from Protvino to ORCA (P2O)." talk at Neutrino GDR Meeting, Paris, November 2017. "<https://indico.in2p3.fr/event/16553/contributions/57491/attachments/45237/56246/P20-zaborov-GDR-neutrino-Nov2017.pdf>", 2017.
- [56] KM3NET collaboration, *Letter of intent for KM3NeT 2.0*, *J. Phys. G* **43** (2016) 084001 [1601.07459].
- [57] KM3NET collaboration, *The KM3NeT Neutrino Telescope and the potential of a neutrino beam from Russia to the Mediterranean Sea*, in *18th Lomonosov Conference on Elementary Particle Physics*, pp. 53–60, 2019, 1803.08017, DOI.
- [58] P. Coloma and P. Huber, *Impact of nuclear effects on the extraction of neutrino oscillation parameters*, *Phys. Rev. Lett.* **111** (2013) 221802 [1307.1243].
- [59] U. Mosel, O. Lalakulich and K. Gallmeister, *Energy reconstruction in the Long-Baseline Neutrino Experiment*, *Phys. Rev. Lett.* **112** (2014) 151802 [1311.7288].
- [60] L. Alvarez-Ruso, Y. Hayato and J. Nieves, *Progress and open questions in the physics of neutrino cross sections at intermediate energies*, *New J. Phys.* **16** (2014) 075015 [1403.2673].
- [61] O. Benhar, P. Huber, C. Mariani and D. Meloni, *Neutrino–nucleus interactions and the determination of oscillation parameters*, *Phys. Rept.* **700** (2017) 1 [1501.06448].
- [62] NuSTEC collaboration, *NuSTEC White Paper: Status and challenges of neutrino–nucleus scattering*, *Prog. Part. Nucl. Phys.* **100** (2018) 1 [1706.03621].
- [63] S. Nagu, J. Singh and J. Singh, *Nuclear Effects and CP Sensitivity at DUNE*, *Adv. High Energy Phys.* **2020** (2020) 5472713 [1906.02190].
- [64] D. K. Singha, M. Ghosh, R. Majhi and R. Mohanta, *Optimal configuration of Protvino to ORCA experiment for hierarchy and non-standard interactions*, *JHEP* **05** (2022) 117 [2112.04876].
- [65] S. Choubey, M. Ghosh and D. Pramanik, *Sensitivity study of Protvino to ORCA (P2O) experiment: effect of antineutrino run, background and systematics*, *Eur. Phys. J. C* **79** (2019) 603 [1812.02608].
- [66] D. Kaur, N. R. K. Chowdhury and U. Rahaman, *Effect of non-unitary mixing on the mass hierarchy and CP violation determination at the Protvino to Orca experiment*, 2110.02917.
- [67] V. A. Kostelecky and R. Lehnert, *Stability, causality, and Lorentz and CPT violation*, *Phys. Rev. D* **63** (2001) 065008 [hep-th/0012060].
- [68] V. A. Kostelecky and M. Mewes, *Lorentz and CPT violation in neutrinos*, *Phys. Rev.* **D69** (2004) 016005 [hep-ph/0309025].
- [69] J. S. Diaz, V. A. Kostelecky and M. Mewes, *Perturbative Lorentz and CPT violation for neutrino and antineutrino oscillations*, *Phys. Rev. D* **80** (2009) 076007 [0908.1401].

- [70] A. Kostelecky and M. Mewes, *Neutrinos with Lorentz-violating operators of arbitrary dimension*, *Phys. Rev.* **D85** (2012) 096005 [[1112.6395](#)].
- [71] J. S. Diaz and A. Kostelecky, *Lorentz- and CPT-violating models for neutrino oscillations*, *Phys. Rev. D* **85** (2012) 016013 [[1108.1799](#)].
- [72] J. S. Diaz, *Correspondence between nonstandard interactions and CPT violation in neutrino oscillations*, [1506.01936](#).
- [73] T. Kikuchi, H. Minakata and S. Uchinami, *Perturbation Theory of Neutrino Oscillation with Nonstandard Neutrino Interactions*, *JHEP* **0903** (2009) 114 [[0809.3312](#)].
- [74] S. K. Agarwalla, S. S. Chatterjee and A. Palazzo, *Degeneracy between θ_{23} octant and neutrino non-standard interactions at DUNE*, *Phys. Lett. B* **762** (2016) 64 [[1607.01745](#)].
- [75] M. Masud, S. Roy and P. Mehta, *Correlations and degeneracies among the NSI parameters with tunable beams at DUNE*, *Phys. Rev. D* **99** (2019) 115032 [[1812.10290](#)].
- [76] P. Huber, M. Lindner and W. Winter, *Simulation of long-baseline neutrino oscillation experiments with GLOBES (General Long Baseline Experiment Simulator)*, *Comput. Phys. Commun.* **167** (2005) 195 [[hep-ph/0407333](#)].
- [77] P. Huber, J. Kopp, M. Lindner, M. Rolinec and W. Winter, *New features in the simulation of neutrino oscillation experiments with GLOBES 3.0: General Long Baseline Experiment Simulator*, *Comput. Phys. Commun.* **177** (2007) 432 [[hep-ph/0701187](#)].
- [78] J. Kopp, *Efficient numerical diagonalization of hermitian 3×3 matrices*, *Int. J. Mod. Phys.* **C19** (2008) 523 [[physics/0610206](#)].
- [79] J. Kopp, M. Lindner, T. Ota and J. Sato, *Non-standard neutrino interactions in reactor and superbeam experiments*, *Phys. Rev.* **D77** (2008) 013007 [[0708.0152](#)].
- [80] DUNE collaboration, *Experiment Simulation Configurations Used in DUNE CDR*, [1606.09550](#).
- [81] KM3NET collaboration, *Letter of Intent for KM3NeT2.0*, [1601.07459](#).
- [82] P. Huber, M. Lindner and W. Winter, *Superbeams versus neutrino factories*, *Nucl. Phys.* **B645** (2002) 3 [[hep-ph/0204352](#)].
- [83] G. L. Fogli, E. Lisi, A. Marrone, D. Montanino and A. Palazzo, *Getting the most from the statistical analysis of solar neutrino oscillations*, *Phys. Rev.* **D66** (2002) 053010 [[hep-ph/0206162](#)].
- [84] M. Gonzalez-Garcia and M. Maltoni, *Atmospheric neutrino oscillations and new physics*, *Phys.Rev.* **D70** (2004) 033010 [[hep-ph/0404085](#)].
- [85] R. Gandhi, P. Ghoshal, S. Goswami, P. Mehta, S. U. Sankar and S. Shalgar, *Mass Hierarchy Determination via future Atmospheric Neutrino Detectors*, *Phys. Rev.* **D76** (2007) 073012 [[0707.1723](#)].
- [86] X. Qian, A. Tan, W. Wang, J. J. Ling, R. D. McKeown and C. Zhang, *Statistical Evaluation of Experimental Determinations of Neutrino Mass Hierarchy*, *Phys. Rev.* **D86** (2012) 113011 [[1210.3651](#)].